
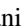
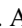




Multiband flattening and linear Dirac band structure in graphene with impuritiesS. Ahmadvhani ¹, M. Alihosseini ¹, S. Ghasemi ¹, I. Ahmadabadi,² N. Hassani ³, F. M. Peeters,^{4,5} and M. Neek-Amal ^{1,*}¹*Department of Physics, Shahid Rajaee Teacher Training University, 16875-163 Lavizan, Tehran, Iran*²*Joint Quantum Institute, NIST, University of Maryland, College Park, Maryland 20742, USA*³*Department of Chemistry, Razi University, Kermanshah 67149, Iran*⁴*Departamento de Física, Universidade Federal do Ceará, 60455-760 Fortaleza, Ceará, Brazil*⁵*Departement Fysica, Universiteit Antwerpen, Groenenborgerlaan 171, B-2020 Antwerpen, Belgium*

(Received 11 September 2022; revised 7 November 2022; accepted 1 December 2022; published 2 February 2023; corrected 21 February 2023)

Flat bands in the energy spectrum have attracted a lot of attention in recent years because of their unique properties and promising applications. Special arrangement of impurities on monolayer graphene are proposed to generate multiflat bands in the electronic band structure. In addition to the single midgap states in the spectrum of graphene with low hydrogen density, we found closely spaced bands around the Fermi level with increasing impurity density, which are similar to discrete lines in the spectrum of quantum dots, as well as the unusual Landau-level energy spectrum of graphene in the presence of a strong magnetic field. The presence of flat bands crucially depends on whether or not there are odd or even electrons of H(F) atoms bound to graphene. Interestingly, we found that a fully hydrogenated (fluorinated) of a hexagon of graphene sheet with six hydrogen (fluorine) atoms sitting on top and bottom in consecutive order exhibits Dirac cones in the electronic band structure with a 20% smaller Fermi velocity as compared to the pristine graphene. Functionalizing graphene introduces various C-C bond lengths resulting in nonuniform strains. Such a nonuniform strain may induce a giant pseudomagnetic field in the system, resulting in quantum Hall effect.

DOI: [10.1103/PhysRevB.107.075401](https://doi.org/10.1103/PhysRevB.107.075401)**I. INTRODUCTION**

One of the most intriguing topics of condensed-matter physics is the emergence of a flat band (FB) in the electronic band structure of two-dimensional (2D) materials [1–7]. The flat bands emerged in a large class of lattices (e.g., kagome and pyrochlore lattices) which are dispersionless (flat) energy bands in the single-particle spectrum [2,8,9]. In fact, the flat bands correspond to completely localized states in a finite volume of the lattice [10–12]. The quenched kinetic energy of electrons due to FBs near the Fermi level, promotes interactions between electrons and facilitates charge transfer between the substrate and the adsorbent [13–15]. These FBs demonstrate exclusive properties, such as narrow width, large effective mass of electrons, very high photoemission intensity, large electron-phonon coupling, and sharp density-of-state (DOS) peaks near the Fermi level [16,17]. Systems containing FBs in their electronic band structure exhibit interesting properties including superconductivity [18], emergent ferromagnetism [19], quantized magnetotransport [20], etc.

There are different ways to manipulate the electronic band structure and introduce a FB into 2D materials, such as by introducing defects [21] and impurities, such as hydrogen (H) [11,12,22], oxygen (O) [15,23], hydroxyl (OH) [12,15,23], fluorine (F) [11,24], and adsorption of a NO molecule [25]. It was found that covalently bound impurities, such as hydroxyl groups, can induce midgap states

in graphene [11,12]. The midgap states are closer to either the valence or conduction band and, thus, are a mixture of them [26]. The density of midgap states controls many electronic properties of the material. Usually, midgap states are generated by coordination defects or the presence of dangling bonds [27,28]. For instance, it is also known that insertion of alkali and alkaline-earth metals into 2D materials can increase the carrier concentration and DOS at the Fermi energy [29,30]. FBs can especially be studied by angle-resolved photoemission spectroscopy (ARPES). For example, the FBs in 1T-VSe₂ and five-layer graphene on the deposited 3C-SiC was studied using ARPES [31,32].

The most well-known example of real 2D materials with FB (or almost FBs) is the magic-angle-twisted bilayer graphene [33,34]. Here the formation of a FB is accompanied by a broad variety of strongly correlated effects and electronic phase transitions, including unconventional superconductivity [35,36]. Another example is a single layer of InSe where a nearly flat hole band appears without twisting. The appearance of this band is associated with an atypical strong electron-phonon interaction and proximity to ferromagnetic and charge-density-wave instabilities [37]. In addition to defected graphene, graphene with impurities can have FBs in their electronic spectra [11,12,38].

A graphene-based counterpart completely functionalized by hydrogen atoms [39], i.e., graphane, is a simple case to study the effect of impurities and their arrangement on electronic properties. Graphane was theoretically investigated by Sofo and co-workers [40] and later experimentally realized by Elias *et al.* [41]. In graphane compared to graphene, carbon

*mehdi.neekamal@gmail.com

hybridization is changed from sp^2 to sp^3 , resulting in an insulator with a band gap of 4 eV [42–44]. Also, it is demonstrated that partially hydrogenated graphene is a semiconductor with variable band gaps [22,44]. Therefore, the C/H ratio and the distribution of H atoms on hydrogen-functionalized graphene are important factors that can affect its electronic properties, such as conductivity and electronic band structure [43,45]. For example, recently, Li *et al.* showed that there are two nontrivial isolated FBs that appear around the Fermi level for a graphene containing a special arrangement of hydrogens [46]. Interestingly, their introduced isolated FBs are similar to those they have found for the interlocking-circles lattice. In most cases, FBs are located in a small part of the reciprocal lattice which appear as a consequence of special lattice geometry and destructive quantum interference.

In this paper, we focus on the physics of graphene monolayer (MLG) having different functional groups, such as H, OH, and F. By using density functional theory calculations, we systematically investigated the electronic band structure and the effect of distribution of the functional groups (O, F) on the electronic properties of graphene. Hydrogenated structures are presented in the main text, whereas the results of other functional groups are reported in the Supplemental Material (SI), Ref. [47]. In particular, we report on multiflat bands, uncrossing (isolated) bands, and Dirac-like bands for hydrogenated (fluorinated) graphene. Also, despite the common believe, in the last part of our paper we show that adding guest atoms do not necessarily destroy the Dirac cone in the spectrum of graphene.

II. COMPUTATIONAL DETAILS

First-principles calculations are performed to study the electronic properties of hydrogenated and fluorinated graphenes. The generalized gradient approximation (GGA) approximation with the Perdew-Burke-Ernzerhof (PBE) exchange-correlation (XC) functional are used for all calculations as implemented in the QUANTUM ESPRESSO package. The cutoff for plane-wave kinetic energy and charge density is taken to be 50 and 500 Ry, respectively. Total energy convergence threshold is set to be 10^{-6} eV. A vacuum of 15 Å is inserted along the z axis to eliminate interactions between the graphene layer's images in the presence of the periodic boundary condition (PBC). After the convergence test, a $6 \times 6 \times 1$ \mathbf{k} -point mesh with Gaussian smearing of 0.01 Ry is used for the Brillouin zone integration in wave-vector space in all of our simulations except for the non-self-consistent calculations.

In studying the electrical conductivity, Boltzmann theory [48,49] is an appropriate tool to gain insight into the transport properties of real materials. In this theory, the electric current is expressed in terms of the conductivity tensor and group velocity in the presence of the electric and magnetic fields, which altogether result in the conductivity tensor. The BOLTZTRAP package is used to calculate the conductivity tensor. This program calculates semiclassical transport based on all electron pseudopotentials which applies the linearly augmented plane-wave method within the framework of the QUANTUM ESPRESSO package. Also, an energy broadening of 0 meV is used in the calculations.

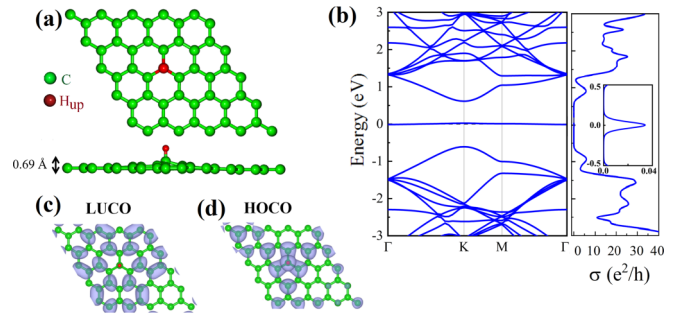


FIG. 1. (a) Partially functionalized graphene with one hydrogen atom in a 5×5 computational unit cell and (b) left: corresponding electronic band structure, and right: electronic conductivity. The inset is a zoom-in of the electronic conductivity around the Fermi level. (c) and (d) Electron distribution of the lowest unoccupied crystal orbital (LUCO) and the highest occupied crystal orbital (HOCO) with a top and side views.

Moreover, molecular dynamics (MD) simulations were carried out under PBCs using GULP molecular simulation software developed by Gale [50] and Gale and Rohl [51]. We have used the reactive force field of ReaxFF [52] in all MD simulations. This semiquantum molecular mechanics force field, i.e., ReaxFF, can satisfactorily elucidate the process of bond formation and bond breaking along with the charge transfer between interacting atoms. The data from experiments and quantum mechanics (QM) are usually used to parametrize the ReaxFF where the parameters are obtained by fitting the data to a training set. Reaction energies and the reaction barriers can be accurately obtained using the ReaxFF method. This feature makes ReaxFF unique as compared to the other reactive force fields. Also, the ReaxFF method is faster than QM-based simulations because it allows simulating chemical reactions of a system on a larger scale ($\gg 1000$ atoms). The combination of low computational cost together with the accurate energies makes the ReaxFF method suitable in the simulation of complex reacting systems. The ReaxFF parameters employed in this paper are from previously published papers [52–54]. Moreover, the MD simulations were performed for a constant number of particles and volume and at room temperature.

III. RESULTS AND DISCUSSION

A. A midgap state

Different configurations of functionalized MLGs with various functional groups provide remarkable band structure with unique properties. As a standard example, when a hydrogen atom is absorbed [11], one of the unpaired electrons in the resonance structure forms a new bond with a hydrogen atom, and the other remains unpaired [see Fig. 1(a)]. The latter electron is delocalized on a broader lattice area. In general, by H chemisorption of carbon atoms, the hybridization remains sp^2 . Here, we considered other conditions which can lead to sp^3 hybridization and a possible gain in the chemisorption of the impurities. Here, we revisit functionalized graphene with

TABLE I. The bond lengths of functionalized graphene with different numbers of hydrogen atoms corresponding to the figures. Significant changes happen in the C-C-H and C-C-C (n) angles. Here, “ n ” and “ f ” represent the next- and far from the functionalized regions, respectively. C^H refers to a carbon atom bonded to a hydrogen atom. The used cell in the calculations is 5×5 which contains 50 carbon atoms.

#H	C – C(f)	C – C(n)	C^H – C	C^H – C^H	C – H	\angle CCH	\angle CCC(n)	\angle CCC(f)
1 [Fig. 1(a)]	1.42	1.40	1.50	–	1.12	104.60	114.12	119.74
2 [Fig. 2(a)]	1.42	1.41	1.50	1.52	1.12	106.86	110.76	120.36
5 [Fig. 2(e)]	1.42	1.37	1.50	1.54	1.12	107.47	108.00	119.82
6 [Fig. 5(a)]	1.42	1.40	1.49	1.52	1.11	108.07	108.13	120.28
9 [Fig. 3(a)]	1.42	1.40	1.50	1.53	1.11	109.56	108.80	119.94
30 [Fig. 3(e)]	1.42	1.41	1.48	1.50	1.10	110.44	107.85	120.04
46 [Fig. 4(e)]			1.47	1.50	1.13	105.02	111.13	
47 [Fig. 4(c)]			1.47	1.52	1.11	106.63	112.59	
48 [Fig. 4(a)]			1.47	1.51	1.11	106.42	110.38	

hydrogen and other functional groups that result in several split and semiparallel FBs emerging in the spectrum.

Figure 1 illustrates the well-known and simplest feasible scenario in which a hydrogen atom is added to MLG, resulting in a FB close to the Fermi level. The green spheres in the left panels of Fig. 1 represent carbon atoms, and the red sphere indicates a carbon atom that is bound to a hydrogen atom on top of the MLG. In fact, when a hydrogen atom binds to a carbon atom, the π bond of the adjacent carbon atoms are broken, and the corresponding electrons participate in the formation of a C-H bond and the appearance of a FB at the Fermi level.

The electronic conductivity presented in the right panel of Fig. 1(b) is zero in the gap region. The midgap state of zero energy does not contribute to conduction. Other structures having different functional groups and similar electronic band structures are given in the SI [47].

The formation of a C-H bond changes the hybridization of carbon atom from sp^2 to sp^3 . As seen in Figs. 1(c) and 1(d) the LUCO and the HOCO illustrate the distribution of electrons on each atom. The electron distribution in HOCO is concentrated on the hydrogen atom, but in LUCO, it is dispersed throughout the carbons around the hydrogen atom. The transformation of carbon sp^2 hybridization in pristine graphene to the sp^3 hybridization in functionalized graphene causes a change in the bond lengths and corresponding angles [39].

The normal C-C bond length is 1.42 Å in graphene and graphite, and the standard bond angle is 120° . For sp^3 hybridization, the C-C bond length is 1.54 Å, the angle is 109.5° , and the C-H bond length is 1.086 Å. One can see in Table I that for a single hydrogen atom, the C-H bond length is not close to the standard value, and C-C-H and C-C-C angles are between 104.6° – 110.5° and 107.8° – 120° , respectively. Also, the C-C bond length lies in the range of 1.42–1.54 Å. This implies intermediate character of hybridization between sp^2 and sp^3 .

To confirm the thermodynamic stability of the hydrogenated graphene, the systems with different numbers of hydrogen and hydroxyl on both sides of graphene are simulated at finite temperature up to 1 ns. The dimensions of the supercell box are set to $12.3 \times 12.3 \times 15 \text{ \AA}^3$. The size of the simulation box along the z axis was considered long enough (15 Å) which eliminates any overlap between hydrogenated graphene images in the neighboring cells. The time step

and total time in the simulation procedure were taken to be 0.5 fs and 1 ns, respectively. To control the temperature of the system, the Andersen thermostat scheme [55] was utilized. The MD simulations confirm the thermodynamic stability of hydrogenated graphene during a reasonable time of simulations. The corresponding movies can be found in the SI [47].

B. Midgap state and uncrossing bands

By increasing the number of impurities, we will show that different arrangements of functional groups influence the electronic band structure significantly, e.g., a band gap is induced in the band structure, shifting electronic characteristic transits from metal to semiconductor. For instance, as can be seen in Fig. 2(a), there is a gap in the symmetrical electronic band structure when two hydrogen atoms are added on top and bottom of carbon atoms. By adding one more hydrogen atom, two uncrossing bands appear around the Fermi level, and one FB emerges at the Fermi level.

In general, odd numbers of adsorbed H atoms provide a midgap state. As an example, five hydrogen atoms on a carbon hexagon leads to the emergence of a FB at the Fermi level [see Fig. 2(f)]. This FB occurrence is independent of the distance of the hydrogenated carbon atoms from each other, e.g., for three carbon atoms near and far from each other, a FB emerges at the Fermi level [see Figs. S1 (a) and S1(b) in the SI in Ref. [47]]. This is also valid for removing an odd number of hydrogen atoms from fully hydrogenated graphene [see Figs. S(c) and S1(d) in the SI in Ref. [47]].

The electronic conductivity of a functionalized hexagon by two and five hydrogen atoms is presented in the right panels of Figs. 2(b) and 2(f), respectively. There is a negligible conductivity at the Fermi level for the structure having two hydrogen atoms on a hexagon whereas a small peak at the Fermi level is observed for five bonded hydrogen atoms that corresponds to the induced FB. It is shown in Figs. 2(c) and 2(d) that the electron distribution in both HOCO and LUCO is concentrated on the hydrogen atoms.

When five hydrogen atoms are on a hexagon, the electron distribution HOCO is concentrated on the hydrogen atoms, but LUCO is dispersed throughout the carbons around the hydrogen atoms [see Figs. 2(g) and 2(h)]. In fact, when an odd number of hydrogen atoms is located on a hexagon ring,

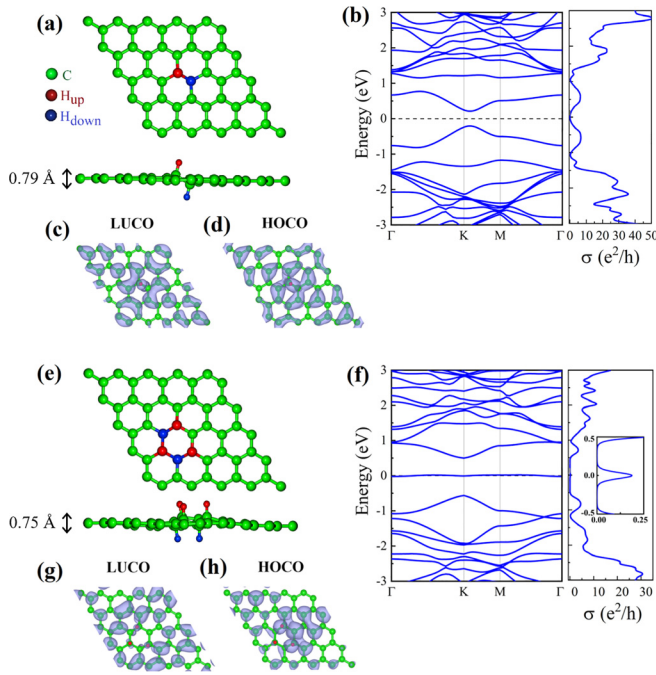


FIG. 2. Partially functionalized graphene with (a) two and (e) five hydrogen atoms in a 5×5 computational unit cell. (b) and (f) Left: the symmetrical band structure and right: electronic conductivity. The inset is a zoom in of the electronic conductivity around the Fermi level. (c), (d), (g), and (h) Electron distribution of LUCO and HOCO, respectively, with top and side view.

this leaves one unpaired electron, resulting in the presence of a FB at the Fermi level.

C. Several avoided crossing bands

The number of FBs around the Fermi level increases as hydrogen atoms are separated leading to the formation of multi- and quasiparallel bands (see Fig. 3). The aforementioned effect depends on the number of unpaired electrons which are separated from each other. These unpaired electrons induce separate FBs around the Fermi level. By increasing the number of functional groups the number of electronic bands around the Fermi level increases. As shown in Fig. 3(a), by adding nine hydrogen atoms the avoided symmetrical crossing bands around the Fermi level increases [Fig. 3(b)]. The corresponding electronic conductivity [right panel of Fig. 3(b)] shows a tiny peak at zero energy corresponding to the induced FBs at the Fermi level.

As the HOCO and LUCO orbitals of this typical configuration in Figs. 3(c) and 3(d) show, the electrons are randomly distributed on the sheet due to the odd number of hydrogen atoms. By increasing further the number of hydrogen atoms and arranging them on carbon atoms, bands are much more flattened around the Fermi level [Fig. 3(f)]. The electronic conductivity in the right panel of Fig. 3(f) exhibits a significant peak which corresponds to energies around the Fermi level because of emerging of almost parallel FBs. LUCO and HOCO orbitals in Figs. 3(g) and 3(h) have complicated patterns and electronic distributions over hydrogen free carbon atoms larger than for the other atoms.

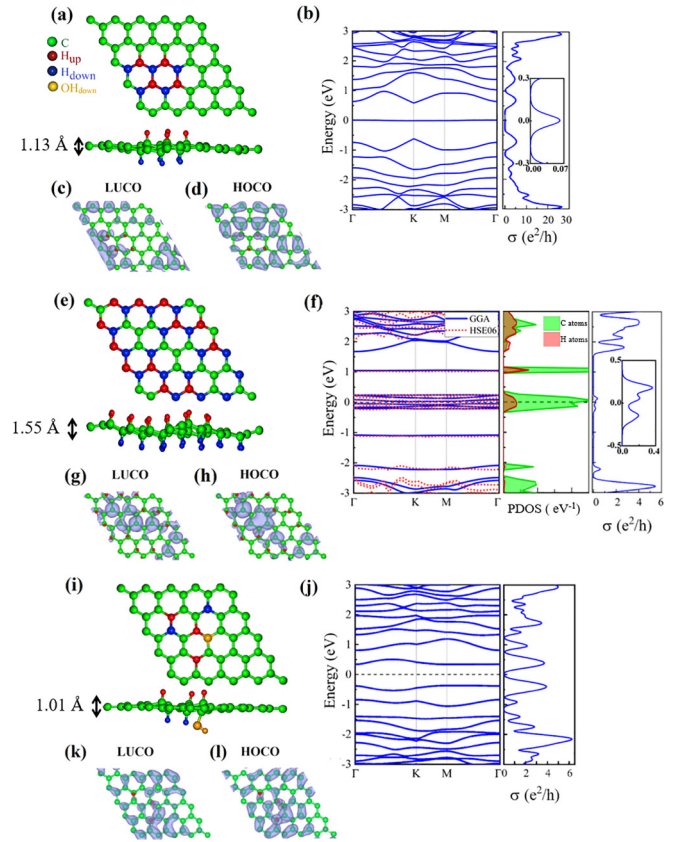


FIG. 3. Partially functionalized graphene with (a) nine and (e) 30 hydrogen atoms and (i) one oxygen and five hydrogen atoms in a 5×5 computational unit cell. (b), (f), and (j) Left: corresponding symmetrical (b), (j) and (f) the multiparallel electronic band structure, and right: electronic conductivity. The insets are a zoom in of the electronic conductivity around the Fermi level. (c), (d), (g), and (h) Electron distribution of LUCO and HOCO, respectively, with top and side view. The colors of each atom are shown in the legend in the left-top corner. For the system (e) we show the partial DOS (PDOS) over C and H atoms and the results of the PSE06 method.

The bond lengths of different sites vary by increasing the number of functional groups. The bond length variations versus the number of functional groups are listed in Table I. The angles and bond lengths of the carbon atoms close to functional groups are significantly altered compared to those far from the functional groups. We added PDOS for the system shown in Fig. 3(f). It is seen most of the contribution is due to the carbon atoms especially those that are the neighbors of carbon-bonding partners of impurities, i.e., $C^H - C$ bonds in Table I [11].

Usually large deformations in graphene can induce strong pseudomagnetic fields [56–58]. By changing functionalized regions a significant nonuniform strain is induced on the MLG. Consequently, a large pseudo-magnetic field can be induced in the system. This is in agreement with the results of Ref. [59] where nonuniform strain distribution in MLG yields giant pseudomagnetic fields causing the emergence of quantum Hall regime. The quantization of energy levels is an important characteristic of the quantum Hall effect, which is observed in the presence of parallel bands around the Fermi

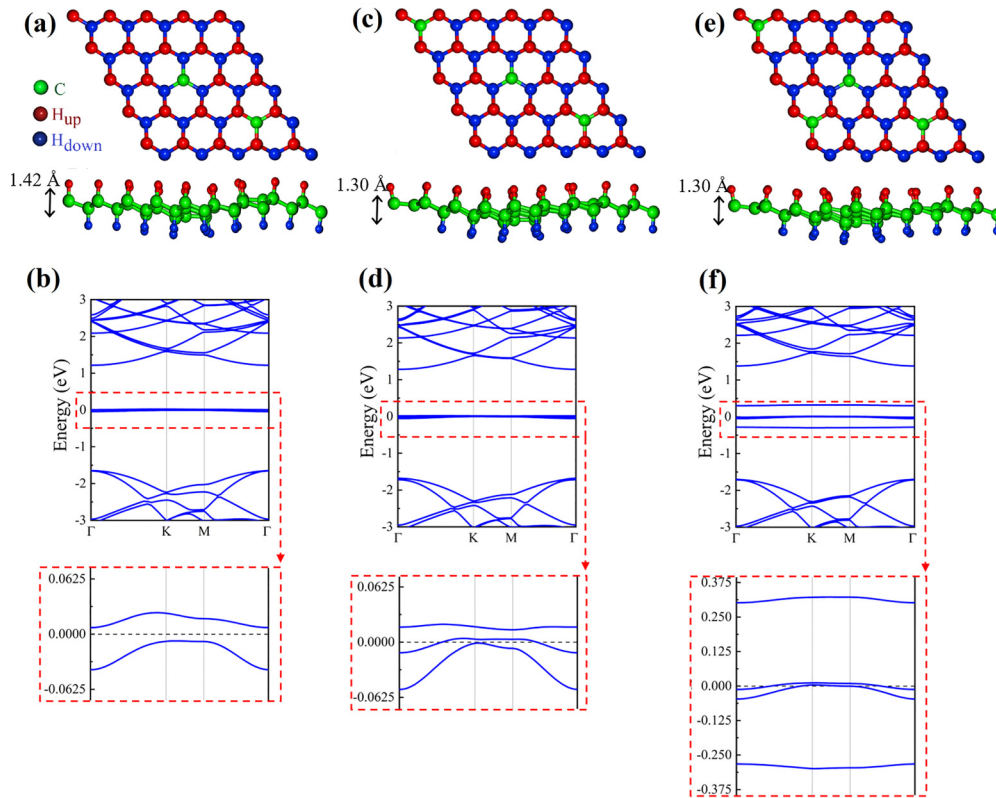


FIG. 4. Fully hydrogenated graphene with (a) and (b) two, (c) and (d) three, and (e) and (f) four carbon atoms without any hydrogen atoms. In their electronic band structures multiflat bands close to the Fermi levels appear. A zoom in of the bands near the Fermi level is shown in the bottom panels.

level as shown in Figs. 3(b) and 3(f). Especially the FBs lies in the interval of $[-300, 300]$ meV around the Fermi level in Fig. 3(f). Surprisingly, two FBs with almost zero width appear at the top and bottom of the Fermi level in the energies $\simeq \pm 1$ eV.

As seen from the conductivity curves [right panels of Figs. 3(b) and 3(f)], the peaks relative to FB energies agree with the results reported for the emerging integer quantum Hall effect in silicene subjected to electric and magnetic fields. Another interesting result was found when we added a $-OH$ group in a system having five hydrogen atoms, i.e., Fig. 3(i). The corresponding band structure is shown in Fig. 3(j) which includes several isolated bands located in the wider range around the Fermi level (see Sec. E below).

Compact percolating states close to the Fermi level are demonstrated in Fig. 4, i.e., overlapping bands around the Fermi level. Such a property appears in fully hydrogenation of the MLG with random hydrogen removal. The number of quasi-FBs at the Fermi level is proportional to the number of missing hydrogen atoms, e.g., for three missed hydrogen atoms, three quasi-FBs appear around the Fermi level.

Scanning tunneling microscopy and atomic force microscopy have proven to be two common methods of excellence for manipulating atoms and molecules one at a time on surfaces [60]. The latter methodologies are almost impossible for depositing light atoms over surfaces, and the corresponding stoichiometric derivatives are difficult to achieve. For instance, monolayer chemical-vapor-deposited graphene is hydrogenated by indirect hydrogen plasma [44],

and graphene membranes on Quantifoil can be exposed to XeF_2 at $70^\circ C$ to obtain fluorinated raphene [61]. On one hand, it is known that the adsorption, e.g., H, O, and F atoms, over graphene is due to a random process where the position of adsorbed atoms is almost out of control whereas the concentration of hydrogen atoms is controllable by controlling the time of exposure [61]. On the other hand, the adsorption of light atoms over both sides of graphene makes the system more stable. In our paper, we put H atoms on the random sites of both sides of graphene [see Figs. 3(e) and 3(f)] and showed that the quasiparallel bands are formed in the spectrum. Note that because in a real situation the low concentration (e.g., graphene fluorinated only for a few hours leads to partially fluorinated graphene) is possible [61], the reported results in Figs. 1(a) and 2(a) can also be experimentally realized. Therefore, both in a low and a high concentration of added atoms, flat bands and corresponding band-gap tuning might be observable [44].

D. Crossing bands at the Dirac point

Now we turn our attention to a special case of hydrogenated (fluorinated) graphene where a Dirac cone in the band structure of graphene with impurity emerges. The common belief is that any kind of adsorption of functional groups over graphene will destroy the Dirac-cone nature of the band structure, or split the bands, opens up a gap, and may generate either midgap states or FBs. However, we found that if one hexagon of graphene is fully hydrogenated (fluorinated), the

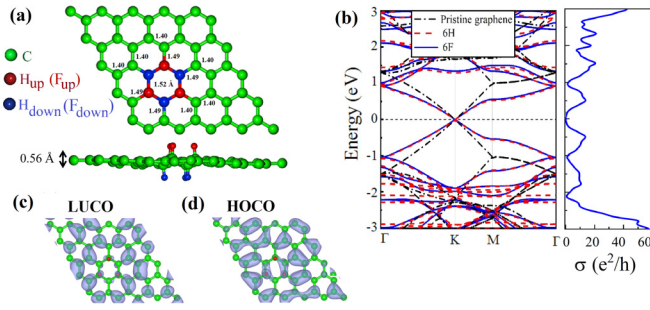


FIG. 5. (a) Partially functionalized graphene with six hydrogen (fluorine) atoms that have only single hexagon rings. In the caption, carbons functionalized with F and H atoms are represented by the same balls. (b) Left: corresponding electronic band structure (black solid lines), red dashed lines represent the pristine graphene electronic band structure. (b) Right: represents electronic conductivity. (c) and (d) Electron distribution of LUCO and HOCO, respectively, with top and side view. The C-C bond lengths inside the central hexagon and around it are given close to each bond.

crossing bands feature of pristine graphene and its low-energy spectrum remains unchanged, and only the Fermi velocity (V_F) is changed. As is obvious from Fig. 5(b), the Fermi velocity (V'_F) is smaller than the standard V_F of pristine graphene, i.e., $V'_F/V_F \approx 0.8$.

In other words, the gap in the band structure is fully closed when hydrogen atoms bond with the carbon atoms of a hexagon of graphene as illustrated in Fig. 5. Interestingly, for this particular arrangement of impurities, the pure graphene band structure is recovered. As depicted in Fig. 5(b), the dashed-solid lines in the left panel represent the band structure of the functionalized graphene with six hydrogen (fluorine) atoms. There is a Dirac point at K similar to the pristine graphene electronic band structure. The electronic conductivity is also illustrated in the right panel of Fig. 5(b).

The C-C bond lengths of the central hexagon are 1.52 Å, the nearest-neighbor C-C bonds around the central hexagon are 1.49 Å and the next-nearest ones are 1.40 Å. The rest of the bonds far from the center have usual lengths, i.e., 1.42 Å. Therefore, the bond lengths in the central and nearest-bond lengths are 7% and 5% stretched with respect to the C-C bond lengths in a pristine graphene. Also the difference between two heights of carbon atoms in the A and B sublattices (containing one up and the other down hydrogen atoms) in the central hexagon is about 0.5 Å which are very close to that of fully hydrogenated graphene (i.e., 0.51 Å) [62].

From orbital properties of the structure, we can observe that LUCO and HOCO are similar to pristine graphene except for regions close to the hydrogen atoms. Note that the next-neighbor hopping between pure carbon atoms around the ring for the graphene hosting a hexagon ring of hydrogens in the origin of the gapless band diagram is impossible (see Fig. 5). This is due to the fact that the electronic density of HOCO and LUCO orbitals of next-neighbor carbon atoms around the hexagon impurity ring do not overlap to create a possible next-neighbor hopping.

As is depicted in the electronic density in Fig. 2(b), carbon atoms adjacent to the two carbon atoms with impurity next to each other can have next-neighbor hopping. The latter is due

to the electronic density overlap between these carbons which is facilitated by the hydrogenated carbon atoms. Since carbon is slightly more electronegative than hydrogen, this overlap is facilitated by more electronic density on the hydrogenated carbon atoms where they act as a bridge between the next-neighbor carbon atoms. Due to the higher electronegativity of fluorine compared to hydrogen and carbon, the hexagon ring hosting fluorine atoms also results in the same gapless system as the next-neighbor hopping here, which is even more difficult to happen compared to the hydrogen impurity. However, as seen from Fig. 5(b) the crossing bands for both hydrogenated and fluorinated graphene are almost the same.

It is worthwhile to mention that, applying uniaxial strain on graphene does not open a gap [63] which is similar to what happens in this case, i.e., a complete symmetry of the induced strain in the system by adsorption of six H or F over a hexagon does not either open a gap. To make sure about the accuracy of the results of the GGA-PBE XC functional, for the band structures, we further checked the spectrum of the system shown in Fig. 3(e) with the screened Coulomb potential hybrid HSE06 [64] [see the dashed line in the band structures of Fig. 3(f)]. Also using HSE06 XC we found a gapless band structure for the system Fig. 5(a) (see Fig. S4 in the SI of Ref. [47]). Therefore, the emergence of the Dirac cone in the electronic structure of the systems is independent of the chosen method.

E. Adsorption of other functional groups (O and F)

For other atoms adsorbed on graphene, such as O and F in the presence of H atoms, the results are presented in Figs. S2 and S3 in the SI in Ref. [47]. As mentioned above, two uncrossing FBs appear around the Fermi level for the structures containing two carbon atoms located far and near from each other whereas hydrogenated by an H atom [see Figs. 2(a) and S2(a) in the SI in Ref. [47]]. By adsorbing an O or F atom on the next-neighbor carbon atom of two bonded and hydrogenated carbon atoms, the previous two bands disappear, and a new nearly FB emerges at the Fermi level. We found that, regardless of the type of functional groups, as the distance between functionalized carbon atoms increases, the number of bands that appear around the Fermi level increases, which is directly related to the number of functional groups. However, as the number of functional groups increases and, consequently, the distance between them decreases, the description of the band structure becomes more complicated. Of particular interest is the spectrum shown in Fig. 3(j) where one oxygen and five hydrogen atoms are adsorbed, and several uncrossing bands are formed in the band structure. It would be worth mentioning that such uncrossing bands appear in the solution of standard one-dimensional potentials, such as Kronig-Penney and Mathieu potentials [65]. Moreover, a quantum dot system for the lowest states has quasiparallel bands which are closely spaced around the Fermi level. On one hand, the band structure of the system shown in Fig. 3(j) around the Fermi level is similar to what is seen in the spectrum of a quantum dot system. On the other hand, using scanning tunneling spectroscopy measurement, distinct Landau-level spectra, and corresponding level-splitting phenomena were observed in graphene layers subjected to strong

magnetic field (12 T) [66,67]. The reported level-splitting phenomena in our paper originated to the change caused by the added atoms and corresponding bond lengths. The investigation of the anomalous quantum Hall effect in our system demands further study. This system can be characterized as a semiconductor with several low-energy flat bands with a gap of about 0.8 eV.

Considering the Dirac dispersion around the so-called K point for the superlattice of graphene with hexagonal impurities shown in Fig. 5, it is known that the Landau energy level dispersion for the graphene is $E_n = \pm \frac{\hbar v_F}{l_B} \sqrt{2|n|}$ [68] where n is the level number and $l_B = \sqrt{\frac{\hbar}{eB}}$. For the graphene with hexagonal impurities, we need to substitute the Fermi velocity that corresponds to the slope of Dirac dispersions for H and F impurities as illustrated in Fig. 5(b) V'_F . As seen from E_n , the Landau levels of the system with impurities have spacing between energies that correspond to the square root of the index of Landau level n . Therefore, because $V'_F/V_F \approx 0.8$, the Landau levels become closer in higher energies.

Eventually, it has been experimentally shown that strain can induce a pseudomagnetic field on the order of 10 T in the monolayer of graphene, paving the way for robust electronics and valleytronics performances. The latter can be achieved because of the spatial and spectral separations of the states in different valleys where the resulting bulk valley polarization is not affected by the short-range scattering [69,70]. Furthermore, it is studied that in periodically strained graphene that is close to the systems considered in the paper, huge pseudomagnetic fields on the order of 100 T can be achieved where more than an order of magnitude decrease in the relaxation of

hot carriers has been reported [71]. Therefore, the flat bands introduced here may be considered as pseudo-Landau levels created by an impurity-induced magnetic field. As a result, integer and fractional quantum Hall phases might be explored for the graphene with impurities introduced in this paper.

IV. CONCLUSIONS

In functionalized graphene, the C-C bond lengths and distribution of impurities in special configurations, has a similar effect as applying nonuniform strains. The electronic conductivity peaks associated with these strain-induced parallel bands are identical to those seen in quantum Hall systems under giant pseudomagnetic fields. Adsorbing an odd number of impurities, such as H, F, and O in the computational unit cell induces a FB around the Fermi level in the band structure due to an unpaired electron. Investigation of low unoccupied crystal band orbitals for different hydrogen configurations illustrates how the electronic distribution contributes in forming a FB which are split and uncrossing of bands around the Fermi level. This FB causes a peak in the electronic conductivity. We found that increasing the number of far-distance impurities results in multiband flattening around the Fermi level. Interestingly, adsorption of six hydrogen and fluorine atoms on a hexagon ring of carbon atoms, reproducing crossing Dirac point at the K point which is similar to the pristine graphene band structure.

ACKNOWLEDGMENTS

N.H. and S.A. acknowledge ISEF support. We acknowledge fruitful comments and help by Z. Javdani.

-
- [1] L. Zheng, L. Feng, and W. Yong-Shi, *Chin. Phys. B* **23**, 077308 (2014).
 - [2] D. Leykam, A. Andreanov, and S. Flach, *Adv. Phys.: X* **3**, 1473052 (2018).
 - [3] S. Pathak, T. Rakib, R. Hou, A. Nevidomskyy, E. Ertekin, H. T. Johnson, and L. K. Wagner, *Phys. Rev. B* **105**, 115141 (2022).
 - [4] L.-H. Tong, Q. Tong, L.-Z. Yang, Y.-Y. Zhou, Q. Wu, Y. Tian, L. Zhang, L. Zhang, Z. Qin, and L.-J. Yin, *Phys. Rev. Lett.* **128**, 126401 (2022).
 - [5] L.-J. Yin, L.-H. Tong, Y.-Y. Zhou, Y. Zhang, Y. Tian, L. Zhang, L. Zhang, and Z. Qin, *Phys. Rev. B* **105**, L201405 (2022).
 - [6] C. Bao, H. Zhang, X. Wu, S. Zhou, Q. Li, P. Yu, J. Li, W. Duan, and S. Zhou, *Phys. Rev. B* **105**, L161106 (2022).
 - [7] L.-Z. Yang, L.-H. Tong, C.-S. Liao, Q. Wu, X. Fu, Y.-Y. Zhou, Y. Tian, L. Zhang, L. Zhang, M.-Q. Cai *et al.*, *Phys. Rev. Mater.* **6**, L041001 (2022).
 - [8] Z. Li, J. Zhuang, L. Wang, H. Feng, Q. Gao, X. Xu, W. Hao, X. Wang, C. Zhang, K. Wu *et al.*, *Sci. Adv.* **4**, eaau4511 (2018).
 - [9] T. Mizoguchi, H. Katsura, I. Maruyama, and Y. Hatsugai, *Phys. Rev. B* **104**, 035155 (2021).
 - [10] B. Sutherland, *Phys. Rev. B* **34**, 5208 (1986).
 - [11] T. O. Wehling, M. I. Katsnelson, and A. I. Lichtenstein, *Phys. Rev. B* **80**, 085428 (2009).
 - [12] T. O. Wehling, S. Yuan, A. I. Lichtenstein, A. K. Geim, and M. I. Katsnelson, *Phys. Rev. Lett.* **105**, 056802 (2010).
 - [13] D. Wei, C. Zhao, A. Khan, L. Sun, Y. Ji, Y. Ai, and X. Wang, *Chem. Eng. J.* **375**, 121964 (2019).
 - [14] J.-A. Yan and M. Y. Chou, *Phys. Rev. B* **82**, 125403 (2010).
 - [15] M. Alihosseini, S. Ghasemi, S. Ahmadvani, M. Alidoosti, D. Nasr Esfahani, F. M. Peeters, and M. Neek-Amal, *J. Phys. Chem. Lett.* **13**, 66 (2021).
 - [16] M. Kohmoto and B. Sutherland, *Phys. Rev. Lett.* **56**, 2740 (1986).
 - [17] K. Sun, Z. Gu, H. Katsura, and S. Das Sarma, *Phys. Rev. Lett.* **106**, 236803 (2011).
 - [18] D. Marchenko, D. Evtushinsky, E. Golias, A. Varykhalov, T. Seyller, and O. Rader, *Sci. Adv.* **4**, eaau0059 (2018).
 - [19] M. Serlin, C. Tschirhart, H. Polshyn, Y. Zhang, J. Zhu, K. Watanabe, T. Taniguchi, L. Balents, and A. Young, *Science* **367**, 900 (2020).
 - [20] S. Wu, Z. Zhang, K. Watanabe, T. Taniguchi, and E. Y. Andrei, *Nature Mater.* **20**, 488 (2021).
 - [21] M. Vanević, V. M. Stojanović, and M. Kindermann, *Phys. Rev. B* **80**, 045410 (2009).
 - [22] H.-C. Huang, S.-Y. Lin, C.-L. Wu, and M.-F. Lin, *Carbon* **103**, 84 (2016).
 - [23] J.-A. Yan, L. Xian, and M. Y. Chou, *Phys. Rev. Lett.* **103**, 086802 (2009).
 - [24] O. Leenaerts, H. Peelaers, A. D. Hernández-Nieves, B. Partoens, and F. M. Peeters, *Phys. Rev. B* **82**, 195436 (2010).
 - [25] O. Leenaerts, B. Partoens, and F. M. Peeters, *Phys. Rev. B* **77**, 125416 (2008).
 - [26] B. Sachs, T. O. Wehling, M. I. Katsnelson, and A. I. Lichtenstein, *Phys. Rev. B* **94**, 224105 (2016).

- [27] H. D. Nelson, S. O. Hinterding, R. Fainblat, S. E. Creutz, X. Li, and D. R. Gamelin, *J. Am. Chem. Soc.* **139**, 6411 (2017).
- [28] R. V. Meidanshahi, S. Bowden, and S. M. Goodnick, *Phys. Chem. Chem. Phys.* **21**, 13248 (2019).
- [29] S. Ichinokura, K. Sugawara, A. Takayama, T. Takahashi, and S. Hasegawa, *ACS Nano* **10**, 2761 (2016).
- [30] K. Tanigaki, T. W. Ebbesen, S. Saito, J. Mizuki, J. S. Tsai, Y. Kubo, and S. Kuroshima, *Nature (London)* **352**, 222 (1991).
- [31] T. Yilmaz and E. Vescovo, *Phys. Rev. B* **105**, L041101 (2022).
- [32] D. Pierucci, H. Sediri, M. Hajlaoui, J.-C. Girard, T. Brumme, M. Calandra, E. Velez-Fort, G. Patriarche, M. G. Silly, G. Ferro, V. Soulière, M. Marangolo, F. Sirotti, F. Mauri, and A. Ouerghi, *ACS Nano* **9**, 5432 (2015).
- [33] E. Suarez Morell, J. D. Correa, P. Vargas, M. Pacheco, and Z. Barticevic, *Phys. Rev. B* **82**, 121407(R) (2010).
- [34] R. Bistritzer and A. H. MacDonald, *Proc. Natl. Acad. Sci. U.S.A.* **108**, 12233 (2011).
- [35] Y. Cao, V. Fatemi, A. Demir, S. Fang, S. L. Tomarken, J. Y. Luo, J. D. Sanchez-Yamagishi, K. Watanabe, T. Taniguchi, E. Kaxiras *et al.*, *Nature (London)* **556**, 80 (2018).
- [36] Y. Cao, V. Fatemi, S. Fang, K. Watanabe, T. Taniguchi, E. Kaxiras, and P. Jarillo-Herrero, *Nature (London)* **556**, 43 (2018).
- [37] E. A. Stepanov, V. Harkov, M. Rösner, A. I. Lichtenstein, M. I. Katsnelson, and A. N. Rudenko, *npj Comput. Mater.* **8**, 118 (2022).
- [38] M. S. M. de Sousa, F. Liu, F. Qu, and W. Chen, *Phys. Rev. B* **105**, 014511 (2022).
- [39] A. A. Dzhurakhalov and F. M. Peeters, *Carbon* **49**, 3258 (2011).
- [40] J. O. Sofo, A. S. Chaudhari, and G. D. Barber, *Phys. Rev. B* **75**, 153401 (2007).
- [41] D. C. Elias, R. R. Nair, T. Mohiuddin, S. Morozov, P. Blake, M. Halsall, A. C. Ferrari, D. Boukhalov, M. Katsnelson, A. Geim *et al.*, *Science* **323**, 610 (2009).
- [42] T. Sreeprasad and V. Berry, *Small* **9**, 341 (2013).
- [43] B. R. Matis, J. S. Burgess, F. A. Bulat, A. L. Friedman, B. H. Houston, and J. W. Baldwin, *ACS Nano* **6**, 17 (2012).
- [44] J. Son, S. Lee, S. J. Kim, B. C. Park, H.-K. Lee, S. Kim, J. H. Kim, B. H. Hong, and J. Hong, *Nat. Commun.* **7**, 13261 (2016).
- [45] M. Jaiswal, C. H. Yi Xuan Lim, Q. Bao, C. T. Toh, K. P. Loh, and B. Ozyilmaz, *ACS Nano* **5**, 888 (2011).
- [46] S. Li, Y. Xie, and Y. Chen, *Phys. Rev. B* **104**, 085127 (2021).
- [47] See Supplemental Material at <http://link.aps.org/supplemental/10.1103/PhysRevB.107.075401> containing few movies of partially hydrogenated graphene and more details.
- [48] G. K. Madsen and D. J. Singh, *Comput. Phys. Commun.* **175**, 67 (2006).
- [49] J. M. Ziman, *Electrons and Phonons: The Theory of Transport Phenomena in Solids* (Oxford University Press, Oxford, 2001).
- [50] J. D. Gale, *J. Chem. Soc., Faraday Trans.* **93**, 629 (1997).
- [51] J. D. Gale and A. L. Rohl, *Mol. Simul.* **29**, 291 (2003).
- [52] J. D. Gale, P. Raiteri, and A. C. Van Duin, *Phys. Chem. Chem. Phys.* **13**, 16666 (2011).
- [53] A. C. Van Duin, S. Dasgupta, F. Lorant, and W. A. Goddard, *J. Phys. Chem. A* **105**, 9396 (2001).
- [54] M. Aryanpour, A. C. van Duin, and J. D. Kubicki, *J. Phys. Chem. A* **114**, 6298 (2010).
- [55] H. C. Andersen, *J. Chem. Phys.* **72**, 2384 (1980).
- [56] M. Neek-Amal and F. M. Peeters, *Phys. Rev. B* **85**, 195446 (2012).
- [57] M. Neek-Amal and F. M. Peeters, *App. Phys. Lett.* **104**, 173106 (2014).
- [58] M. Neek-Amal, L. Covaci, and F. M. Peeters, *Phys. Rev. B* **86**, 041405 (2012).
- [59] F. Guinea, M. Katsnelson, and A. Geim, *Nat. Phys.* **6**, 30 (2010).
- [60] Y. Sugimoto, P. Pou, O. Custance, P. Jelinek, M. Abe, R. Perez, and S. Morita, *Science* **322**, 413 (2008).
- [61] R. R. Nair, W. Ren, R. Jalil, I. Riaz, V. G. Kravets, L. Britnell, P. Blake, F. Schedin, A. S. Mayorov, S. Yuan *et al.*, *Small* **6**, 2877 (2010).
- [62] S. Costamagna, M. Neek-Amal, J. H. Los, and F. M. Peeters, *Phys. Rev. B* **86**, 041408(R) (2012).
- [63] M. Farjam and H. Rafii-Tabar, *Phys. Rev. B* **80**, 167401 (2009).
- [64] J. Heyd, G. E. Scuseria, and M. Ernzerhof, *J. Chem. Phys.* **118**, 8207 (2003).
- [65] G. Grosso and G. P. Parravicini, *Solid State Physics*, 2nd ed. (Academic, San Diego, 2013).
- [66] G. Li and E. Y. Andrei, *Nat. Phys.* **3**, 623 (2007).
- [67] L.-J. Yin, S.-Y. Li, J.-B. Qiao, J.-C. Nie, and L. He, *Phys. Rev. B* **91**, 115405 (2015).
- [68] A. H. Castro Neto, F. Guinea, N. M. R. Peres, K. S. Novoselov, and A. K. Geim, *Rev. Mod. Phys.* **81**, 109 (2009).
- [69] T. Low and F. Guinea, *Nano Lett.* **10**, 3551 (2010).
- [70] N. Levy, S. Burke, K. Meaker, M. Panlasigui, A. Zettl, F. Guinea, A. C. Neto, and M. F. Crommie, *Science* **329**, 544 (2010).
- [71] Y. Jiang, J. Mao, J. Duan, X. Lai, K. Watanabe, T. Taniguchi, and E. Y. Andrei, *Nano Lett.* **17**, 2839 (2017).

Correction: The affiliation for the first author was presented incorrectly and has been set right. This change necessitated renumbering of the affiliation indicators.